Platelike MFI Crystals with Controlled Crystal Faces Aspect Ratio

Weijiong Dai, Cassandre Kouvatas, Wenshu Tai, Guangjun Wu, Naijia Guan, Landong Li, Valentin Valtchev

Plate-like MFI Crystals with Controlled Crystal Faces Aspect Ratio

Weijiong Dai,[1,2] Cassandre Kouvatas,[2] Wenshu Tai,[1] Guangjun Wu,[1*] Naijia Guan,[1] Landong Li,[1] and Valentin Valtchev[2,3*]

[1] *School of Materials Science and Engineering & National Institute for Advanced Materials, Nankai University, Tianjin 300350, P.R. China*

[2] *Qingdao Institute of Bioenergy and Bioprocess Technology, Chinese Academy of Sciences, 189 Songling Road, Laoshan District, Qingdao, Shandong 266101, P. R. China*

[3] *Laboratoire Catalyse et Spectrochimie, Normandie Univ, ENSICAEN, UNICAEN, CNRS, 6 Boulevard Maréchal Juin, 14050 Caen, France*

Abstract

Zeolite crystals offering a short diffusion pathway through the pore network are highly desired for a number of catalytic and molecule separation applications. Herein, we develop a simple synthetic strategy toward reducing the thickness along *b*-axis of MFI-type crystals, thus providing a short diffusion path along the straight channel. Our approach combines preliminary aging and a fluoride-assisted low-temperature crystallization. The synthesized MFI crystals are in the micron-size range along *a*- and *c*-axis, while the thickness along the *b*-axis is a few tens of nanometers. The synthesis parameters controlling the formation of plate-like zeolite are studied, and the factors controlling the zeolite growth identified. The synthesis strategy works equally well with all-silica MFI (silicalite-1) and its Al- and Ga-containing derivatives. The catalytic activity of plate-like ZSM-5 in the methanol-to-hydrocarbons (MTH) reaction is compared with a commercial nano-sized ZSM-5 sample, as the plate-like ZSM-5 exhibits a substantially extended lifetime. The synthesis of plate-like MFI crystals is successfully scaled up to a kilogram scale.

Keywords: Zeolite; Morphology; Ultra-thin crystals; Catalysis

Introduction

Zeolites are initially discovered as minerals in sediment and pegmatite rocks.[1] Natural zeolites are mainly used in agriculture, water, and soil remediation, while their synthetic counterparts have diverse industrial applications, as heterogeneous catalysis and molecular sieving are the major industrial fields of use.[2,3] More than 40% of acid-catalyzed reactions are currently based on synthetic zeolites.[4] The great success of zeolites in catalysis is related to their unique structural features, i.e., the ordered channels of molecular dimensions and the presence of modulable active sites.[5] However, the narrow channels of zeolite impose a significant restriction on the transport of molecules, causing an increase in the secondary reactions as well as the subsequent catalyst deactivation by coking.[5–8]

The diffusional problems can be partially circumvented by reducing the path length through the zeolite crystal. The two strategies employed to reduce the diffusion path in zeolites are the decrease of the crystals to the nano-sized range[9–12], and the introduction of larger secondary (meso-/macro-) pores in the crystals.[13–15] Zeolites comprising a secondary pore system, which serves as highways for reactants and products, are often called hierarchical, and their preparation is usually complex.[14,16] The synthesis of zeolite nanocrystals also has a downside as the specific synthesis conditions and complex product processing are required.[9] An alternative solution that could solve the problem with the diffusion limitations in zeolites without using additional treatments, as in the case of hierarchical and nano zeolites, is the synthesis of micron-sized zeolites with particular morphology. More precisely, the control of zeolite morphology could be used to limit the growth in the direction along the channel system of interest, thus shortening the diffusion pathway. Tuning zeolite morphology could also allow developing the face where the channel system of interest is presented on the zeolite surface, thus increasing the number of pore opening per unit crystals surface. This strategy is particularly important in preparing zeolites with a biased performance of different channel systems. For instance, MFI-type material, used in various catalytic and separation processes, contains straight and zig-zag channel systems running along *b* and *a* crystal axis, respectively (Figure S1). Shortening the diffusion path along the straight channel (*b*-axis) changes zeolite performance substantially.[17–20]

An ultimate example of this strategy was the preparation of zeolite nanosheets, first prepared by Ryoo

and co-workers.[8] Ryoo's group decreased the thickness of MFI-type zeolite along the *b*-axis to one unit cell. Nanosheet-like zeolites focused zeolite community's attention with remarkable catalytic performance in several reactions,[21–25] and superior separation ability in membrane applications.[20,26,27] However, these zeolitic materials are synthesized by using the complex and expensive structure-directing agents (SDAs),[28–30] or by tedious swelling, pillaring, and exfoliation procedures.[31] The size of the zeolite nanosheet is usually tiny (100-200 nm in length), and the handling is even more complex than the conventional nano-zeolites.

From a practical point of view, the synthesis of zeolite crystals with morphology that enhances the transport through a particular channel system without using an exotic SDA is highly desired. The aspect ratio between different crystal faces should be changed in a way to minimize the length of the channel. Maximizing the face's size where the channel system of interest appears on the crystal surface is also important. Keeping the zeolite crystal size in the micrometer range and decreasing the size to a few tens of nanometers in a particular crystallographic direction has significant practical value. Such crystals can be processed employing the conventional post-synthetic protocols and do not require any additional treatments.

Previously studies have demonstrated that adjusting synthesis parameters or adding synthesis modifiers could substantially change zeolite crystal morphology.[32–37] For instance, long to short prismatic LTL-type crystals were synthesized by simple changing of water content in the synthesis gel.[33] The zeolite Beta morphology was controlled, varying the pH of the system.[35] Crystals with well-developed pyramidal (h0l) or pinacoidal (001) faces were obtained. For instance, at high pH plate-like zeolite Beta with a pinacoidal face dominating crystal morphology was obtained. The use of additives can also effectively tailor the aspect ratio of zeolite crystals. Different types of additives, including alcohol,[38,39] tributylphosphine oxide,[40] graphene oxide,[41] peptoids,[42] and amino acid arginine,[43] were employed to modify crystal morphology of different types of zeolites. Although some positive results were published, a dramatic change in the aspect ratio between different faces was not reported to the best of our knowledge. None of these studies guide how one can tune the crystal morphology to nano-size range in a particular crystallographic direction.

Fluorine ion (F^-) is the alternative OH^- as a mineralizing agent in zeolite synthesis.[44,45] It is usually

used in the synthesis of high- or all-silica zeolites in a quasi-neutral medium. It was reported that fluoride could also be used to achieve the oriented growth of thin zeolite films.[46] Hence, we selected the ammonium fluoride (NH_4F) as a zeolite synthesis modifier to change the crystal face aspect ratio between the faces of the crystals.

The present study aims to obtain ultra-thin zeolite plates, keeping the other crystals dimension in the micron-size range. Fulfilling this goal would provide a relevant approach to zeolites with improved accessibility and decreased diffusion limitations, avoiding the use of complex organic structure-directing agents (SDA) and multi-step procedures. Our approach is exemplified by preparing MFI-type crystals with controllable aspect ratios between different crystal faces. We selected the MFI-type zeolite because it is an industrially relevant zeolite,[47] and exhibits two different channel systems, highlighting the effect of crystal morphology on zeolite accessibility and transport through the channels.

Results and discussion

Substantial preliminary work has been executed to adjust the ratio between different reactants and pre-synthesis aging conditions. The reference, NH_4F-free synthesis, with a molar composition of 0.1 TPAOH: 1.0 SiO_2: 30 H_2O was performed at 90 °C for 72 h under static condition. A highly crystalline product was obtained (Figure S2f). The crystal size was close to 1 µm, as each crystal contained a 90° twin crystal, a morphological feature often observed for the MFI-type material (Figure S3a). The impact of NH_4F on the MFI crystal morphology was studied with a gel of composition 0.1 TPAOH: 1.0 SiO_2: 0.8 NH_4F: 30 H_2O (see Supporting Information for details). This system yielded well-shaped, very thin plate-like crystals. The XRD pattern, Ar physisorption analysis, and representative TEM and SEM images of the crystals are shown in Figure 1. The product was highly crystalline, according to the XRD study (Figure 1a). This result was confirmed by the type I physisorption isotherm, with fast uptake at low relative pressure, characteristic of a zeolite type material (Figure 1b). The micropore volume (0.14 cm^3/g) and specific surface area (430 m^2/g) of the plate-like MFI zeolite crystals are characteristic of highly crystalline MFI-type material (Table S1). The high crystallinity of the single-crystalline plate-like zeolite is also illustrated by the well-defined lattice fringes and the selected area electron diffraction

(SAED) pattern in the HR-TEM image (Figure 1f and 1g). Microscopy study (Figure 1c, 1d and 1e) reveals that crystals' length-width dimensions are in the micron scale. Meanwhile, the thickness of the obtained crystals was ~100 nm. Thus, the crystals are well-shaped with developed (100) and (0kl) faces, while the (010) face is very short. In the enlarged view HAADF-STEM image (Figure 1f), the zeolite channels along the b-axis can be clearly observed.

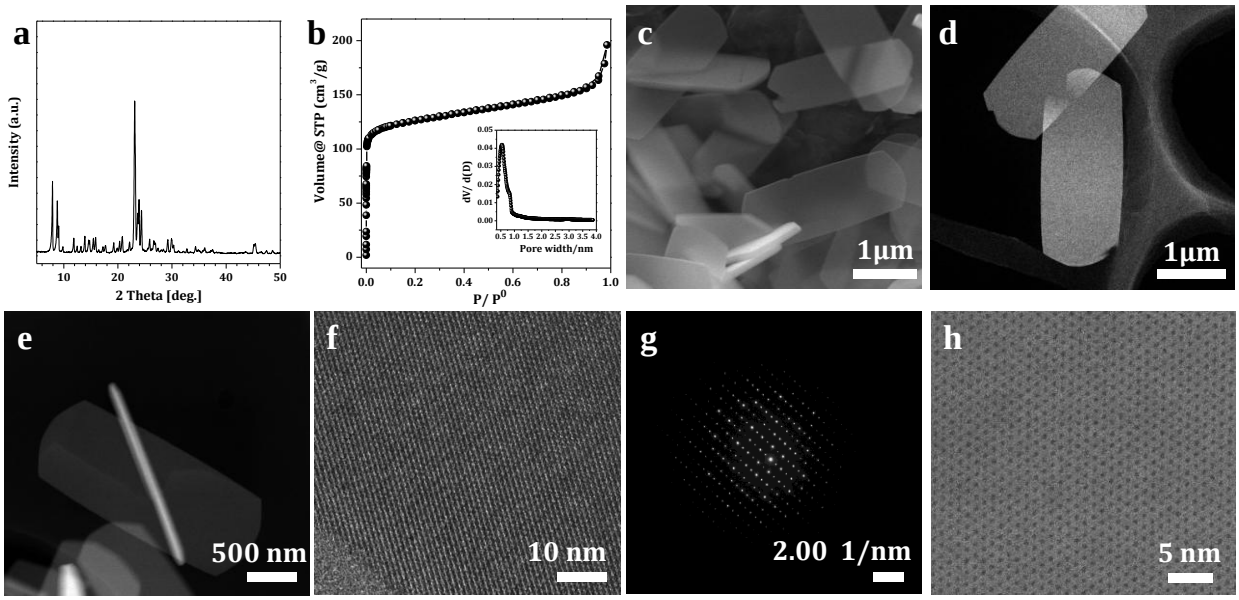

Figure 1. General features of silicalite-1 obtained in the 0.1TPAOH:1.0SiO_2:0.8NH_4F:30H_2O system: (a) XRD pattern of as-synthesized solid products; (b) Ar physisorption isotherm of the calcined product with pore size distribution shown as an inset; (c) SEM and (d, e) low-magnification HAADF-STEM images of silicalite-1 crystals; (f) high-resolution TEM images, (g) the selected area electron diffraction (SAED) pattern; (h) high-magnification HAADF-STEM image of silicalite-1 crystals after calcination.

A systematic study of the ammonium fluoride content on the MFI morphology was performed using the system: 0.1 TPAOH: 1.0 SiO_2: y NH_4F: 30 H_2O, where y was varied between 0 and 1.6. The morphology of twin crystals obtained without NH_4F (Figure S3a) changed gradually with the increase of NH_4F content in the gel. The most noticeable change was the disappearance of 90° twin crystal (Figure S3d). The other significant change was the change of the aspect ratio between (010) and (100) faces. This effect is a consequence of the decrease in the size of (100) face. The increase of y value to 1.2 and 1.6 further accentuated the morphological changes of MFI-type material, as crystal's thickness reached several tens of nanometers (Figure S3e and S3f). Noteworthy, the crystals synthesized in the

NH_4F-containing medium are larger than that of the reference sample. Thus, the silicalite-1 crystals grow from ~700 nm to ~3000 nm along the *c*-axis, at the same time decreasing the thickness from ~500 nm to ~100 nm along the *b*-axis (Figure 2a). These morphological changes are better presented via the aspect ratio between different faces. The ratio between *c*- and *a*-axis (L_c/L_a) as well as between *c*- and *b*-axis (L_c/L_b) was used to evaluate the changes in the (100) and (010) faces, where the pore mouths of zig-zag and straight channel appears on the surface, respectively. The L_c/L_b aspect ratio increased from ~2.5 to ~26, when NH_4F content in the gel changed from 0 to 1.6 (Figure 2c). At the same time, as can be observed from Figure 2b, the change in the L_c/L_a was not dramatic (from ~1.3 to ~2.7), revealing that the growth in *b* direction was greatly affected by the NH_4F addition. The zeolite crystallinity also depends on the NH_4F content in the gel, as can be seen in Figure S2. At low NH_4F content (y = 0.05 and 0.2), an amorphous phase containing a few MFI crystals was observed, even though the crystallization was extended to 168 h (Figure S3b and S3c). In contrast, a highly crystalline product was obtained within 72 h when y increased to 0.8. Further increasing y to 1.2 and 1.6 shortens the crystallization time to 48 h and 24 h, respectively. However, it did not bring substantial change in the crystalline product (Figure S3e and S3f), showing a threshold of NH_4F concentration, after which the morphology is not impacted. The best result in terms of high L_c/L_b aspect ratio and short crystallization time was obtained with y = 0.8. In this case, the average crystal thickness along *b*-axis was ~100 nm, and the crystalline product was obtained within 72 h. The set of experimental results unambiguously shows that the NH_4F concentration has a direct effect on the MFI crystal growth, including both the crystallization kinetics and the crystal morphology.

It should be noted the effect of the 90 °C aging prior to the addition of NH_4F to the gel, which plays a crucial role in the formation of plate-like MFI zeolite crystals. Without this aging step, the gel with a similar molar composition (0.1 TPAOH: 1.0 SiO_2: 0.8 NH_4F: 30 H_2O) did not yield crystalline material up to 168 h crystallization (Figure 2e). In order to get an insight into the 90 °C aging on gel structure, we performed IR analysis. The FTIR spectra of the samples collected after aging at 90 ℃ for 12 h are shown in Figure S4. Compared to the amorphous silica, the sample taken after 12 h exhibits a broad band at ~550-570 cm^{-1}, which reveals that elements of pentasil structure are already present in the solid.[48] Increasing the aging time from 12 to 24 and 36 h changed the growth rate, and thus the

crystallization time was reduced to 72 h, 36 h and 24 h, respectively. However, 90° twin crystals were yielded instead of single plate-like crystals when the aging time was extended to 24 and 36 h (Figure 2e).

It is known that the aging process impacts zeolite nucleation and thus crystal growth.[49] In this work, the aging step was necessary to obtain MFI crystals in the NH_4F containing gel as 12 h was the optimal aging time yielding very thin plate-like crystals. The crystal morphology is impacted by the species generated during the aging process. We anticipate that the plate-like morphology is a consequence of a high concentration of precursors species with similar development and a particular mechanism of oriented aggregation, which leads to the preferential growth along the *a*- and *c*-axis, and results in a highly developed (010) face. However, the intimate mechanism laying behind this particular growth is difficult to be elucidated.

The impact of the SDA content on the crystal morphology was studied using the system: x TPAOH: 1.0 SiO_2: 0.8 NH_4F: 30 H_2O, where x was varied in the range of 0.08–0.35. As shown in Figure S5, with the increase of SDA content, MFI crystals' size decreased. This is the expected effect due to the more abundant nucleation in TPA-rich systems.[11] Meanwhile, a decrease from ~30 to ~20 of the L_c/L_b ratio can be observed when x is below 0.125. After that, no change of the L_c/L_b ratio was detected (Figure S6). However, the L_c/L_a was not influenced too much by the SDA concentration. It remained in the range of 1.8–2.8 (Figure S6). The decrease of the overall crystal dimension resulted in much thinner along *b*-axis crystals. Thus crystallites with an impressive thickness of ~10 nm along the *b*-axis without using any organic modifier were obtained (Figure 2d and S5). These results show that the SDA content has a limited influence on the aspect ratio between different faces. However, the TPAOH content exhibits a noticeable impact on the crystallinity zeolite products, as shown in Figure 2d. For instance, at x = 0.08, the relative crystallinity of 72 h synthesized sample is ~63 %. It can be improved by extending the crystallization time to 120 h (Figure S7). Increasing x from 0.08 to 0.35 led to highly crystalline zeolite crystals, which was obtained within 72 h.

As MFI-type zeolites are often synthesized at elevated temperatures ($T \geq 150\ ^oC$), we have studied the impact of synthesis temperature on the morphology of the plate-like crystals. Noteworthy, plate-like MFI crystals can be obtained over a temperature range of 90–180 ^oC using the system 0.1 TPAOH: 1.0

SiO_2: 0.8 NH_4F: 30 H_2O (Figure S8). As shown in Figure S8 and S9, increasing the crystallization temperature from 90 to 180 ^oC resulted in a slight increase in the crystal size. Thus the length along the *c*-axis changed from ~2600 nm to ~3500 nm, while along the *b*-axis, the increase was only from ~100 nm to ~150 nm. Meanwhile, the length along *a*-axis did not show any obvious change. Consequently, the aspect ratios, L_c/L_a and L_c/L_b, remained nearly unchanged (Figure S9d). Thus the crystallization temperature shows a weak influence on the aspect ratio between different crystal faces. The corresponding relative crystallinity increased from ~85 to ~100%, with the temperature rising from 90 °C to 180 °C (Figure S9a).

Summarizing the set of experimental results, one can state that an aging step of 12 h generating nuclei in the system before the addition of NH_4F is indispensable for the formation of plate-like MFI crystals. Further, with precise control of NH_4F content and tuning the synthesis parameters, single-crystalline plate-like MFI zeolite with adjustable thickness can be obtained (Figure 2).

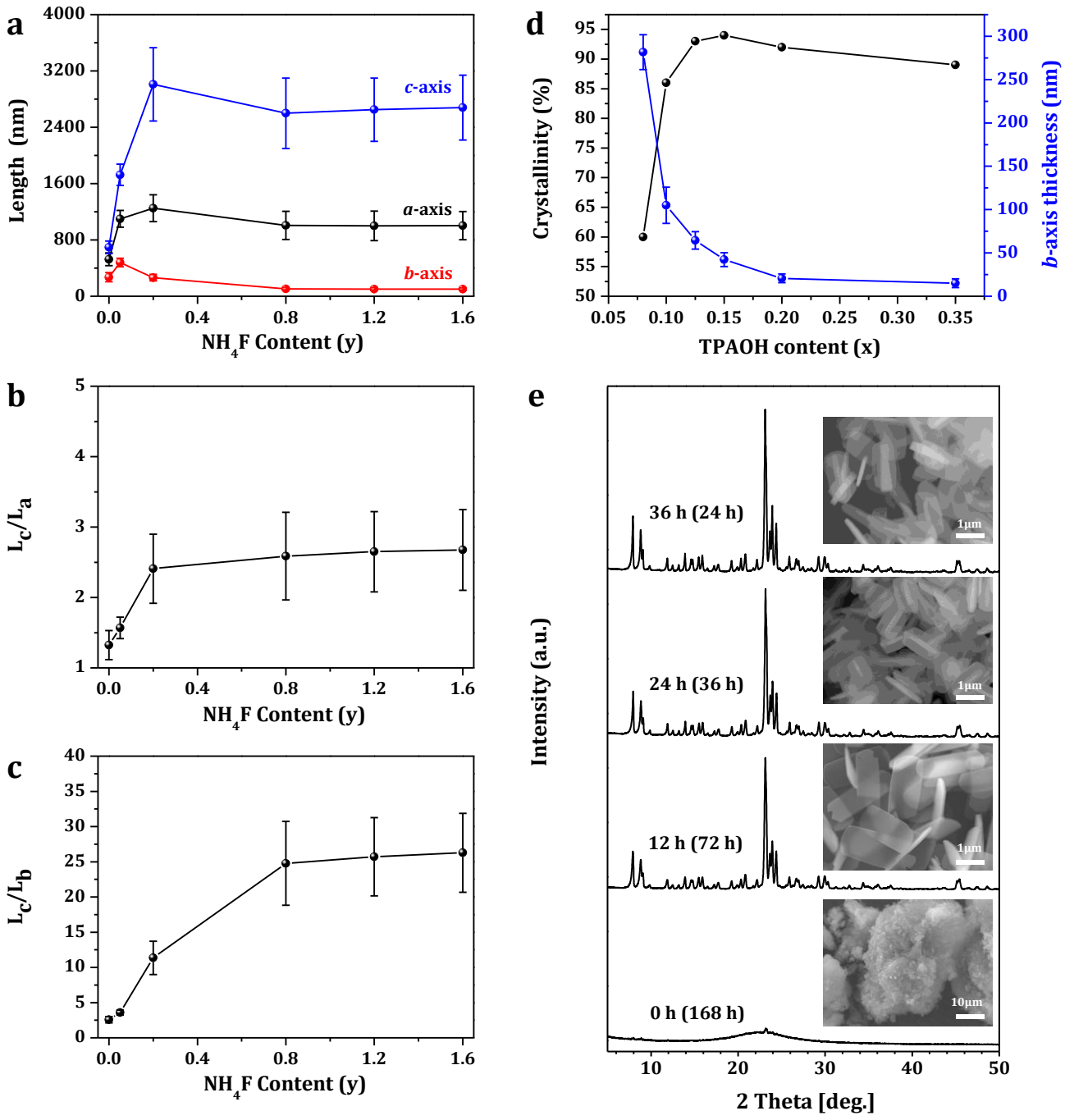

Figure 2. Synthesis parameters relevant to the formation of plate-like MFI zeolite crystals from the synthesis system x TPAOH: 1.0 SiO_2: y NH_4F: 30 H_2O crystallized at 90°C: (a) the length along the three axes; (b) L_c/L_a and (c) L_c/L_b aspect ratios; (d) effects of TPAOH content on the relative crystallinity and *b*-axis thickness of MFI zeolite; (e) XRD patterns of solid products subjected to 0 h, 12 h, 24 h, and 36 h aging time (the crystallization time is shown in parentheses) from the system with x = 0.1, y = 0.8. Inset (e): representative SEM images of solid products.

Mechanism of plate-like MFI crystals formation

The mechanistic analysis of plate-like MFI formation was performed using an all-silica system with molar composition 0.1 TPAOH: 1.0 SiO_2: 0.8 NH_4F: 30 H_2O. The intermediates formed in the course of zeolite synthesis were studied to shed light on the process. As pointed out above, the gel was aged at 90 °C for 12 h, then dissolved NH_4F was added, and the resultant mixture stirred at 90°C for 12 h more. Finally, the synthesis was performed under static conditions at 90 °C for 48 h, as a sample was taken after 3, 6, 9, 12, 16, 24, 36, and 48 h.

The XRD pattern of the 12 h aged gel showed that it is amorphous (Figure S10). After the addition of NH_4F, the first MFI trace, indicated by the characteristic diffraction line at 23.1° Two Theta, appeared after 3 h crystallization. The crystalline phase developed rapidly, and a highly crystalline material was obtained after 48 h synthesis. Meanwhile, the amorphous phase gradually decreased and fully disappeared after 48 h crystallization (Figure S12).

The obtained intermediates, as well as the 12 h aged precursor, were inspected by transmission electron microscopy. After 3 h aging, only bulk, uniform in texture gel particles were observed (Figure S13). No substantial changes in the gel structure were found after 12 h aging (Figure 3a). Upon the addition of NH_4F and 3 h hydrothermal treatment at 90 °C, the gel precursor structure changed dramatically. Bulk gel disintegrated, and small nanometric particles appeared in the system. We attribute this effect to the fluorine ions' mineralizing ability, which breaks the gel structure and reorganizes silica species. Small, 10–20 nm in size isometric particles with oval shape was the only phase observed in the product (Figure S14). The formation of nanoparticles certainly changes the exchange between the solid and liquid phase and contributes to the reaction kinetics in general. We anticipate the structure/chemistry of newly formed upon the fluorine addition nanoparticles contributes to the formation plate-like zeolite crystals. However, we do not have experimental prove supporting our suggestion. These tiny nanoparticles continue existing up to 12 h hydrothermal treatment. However, some changes in their textural organization occur. Namely, the particles agglomerate and built agglomerates with an elongated shape. The individual 10–20 nm nanoparticles are still well distinguishable in the aggregates (Figure 3b). Plate-like particles appear in the solid after 12 h treatment at 90 °C (Figure 3c). According to the XRD study, the solid is still amorphous at this stage (Figure S11). Upon autoclave treatment, the number of

plate-like particles increases, and they evolve into plate-like crystals with the MFI-type morphology. The first XRD trace of MFI-type material is detected after 3 h hydrothermal treatment in the autoclave (Figure S12). With the crystallization time extension, the amount of crystals increases at the expense of the isometric 10–20 nm particles (Figure 3d-f). These data show that the small colloid species with oval shape, observed at the beginning of the crystallization process, serve as nutrients for the crystal growth process. In the last stages of crystals growth (24–48 h), substantial growth of zeolite crystals is observed (Figure 3g-i). At this later stage, there is almost no amorphous phase in the system. Therefore, the growth is a consequence of the Ostwald ripening of the crystals, which does not change crystal morphology. Thus plate-like with very high L_c/L_b aspect ratio MFI crystals are obtained (Figure 3i).

The combined XRD-TEM investigation revealed that the addition of NH_4F and the treatment at 90 °C changed the gel structure substantially. Our interpretation is that the fluoride species break the gel structure, and thus, very small nanoparticles are formed, which form larger agglomerates. First zeolite crystallites are formed during this stage, most probably by the oriented aggregation of precursors particles.[50] We do not have molecular level information of the mechanism leading to the formation of extra-thin MFI-type crystals and the preferential growth along *a*- and *c*-axis leading to the well-developed (010) face. However, we clearly identify the formation of first crystallites during the 90 °C aging prior to the autoclave treatment, as indicated by the splitting of the pentasil vibration at 540~570 cm^{-1} in the FTIR spectra (Figure S4).[51] The autoclave treatment just accelerates the growth rate without altering the growth mechanism. Thus, the particular morphology is a result of the preliminary 90 °C aging of the gel in the presence of NH_4F. On the ground of collected results, the system's evolution leading to plate-like MFI crystals is presented in Scheme 1.

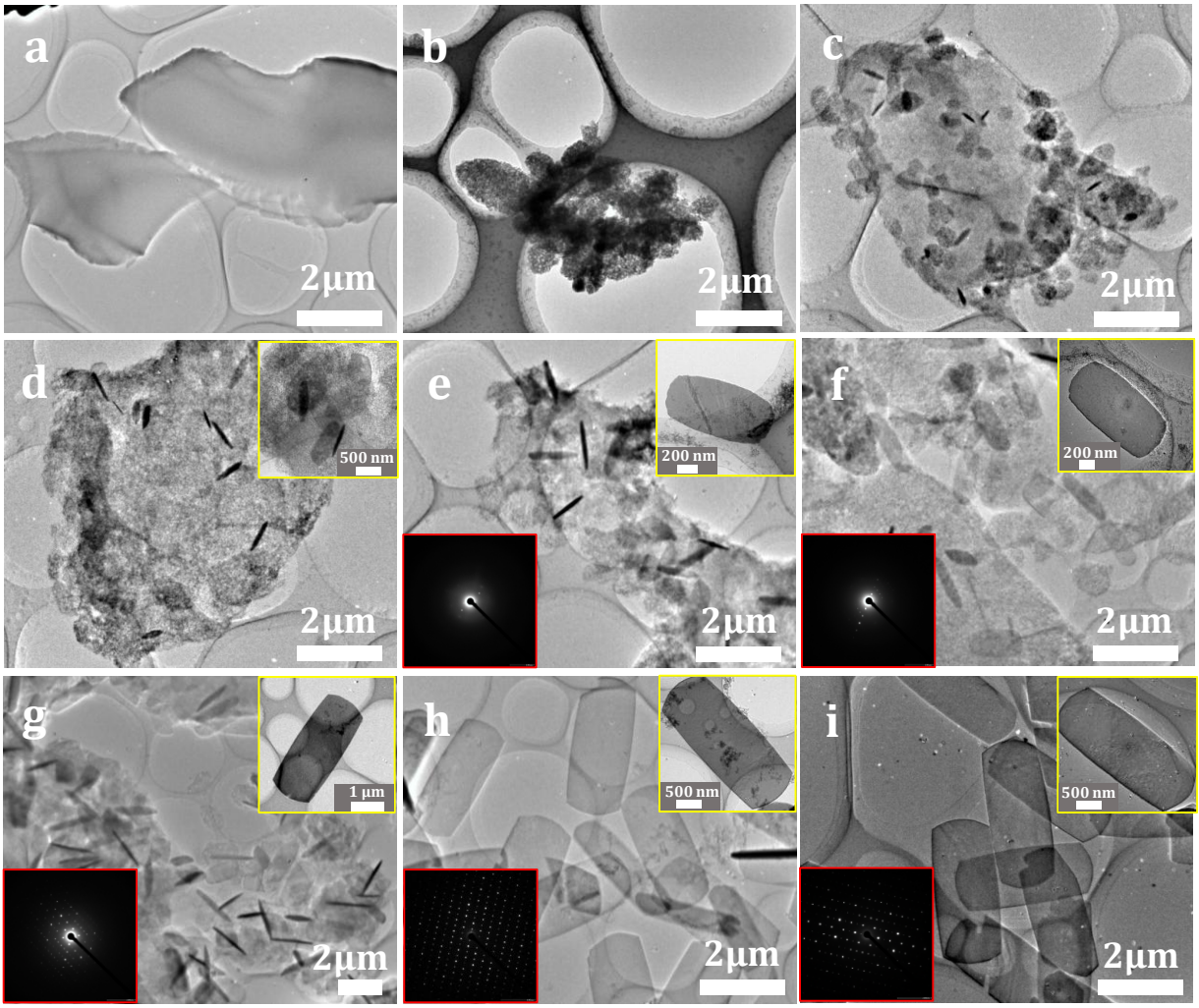

Figure 3. TEM analyses of products at different stages of zeolite synthesis: (a) After aging for 12 h at 90 °C. After the addition of NH_4F and stirring at 90 °C for 6 (b) and 12 h (c). After hydrothermal treatment in the autoclave for 6 (d), 9 (e), 12 (f), 24 (g), 36 (h) and 48 h (i). Scale bar: 2 µm. Insets: views of single plate-like MFI zeolite crystal (marked with yellow) and the selected area electron diffraction patterns (marked with red).

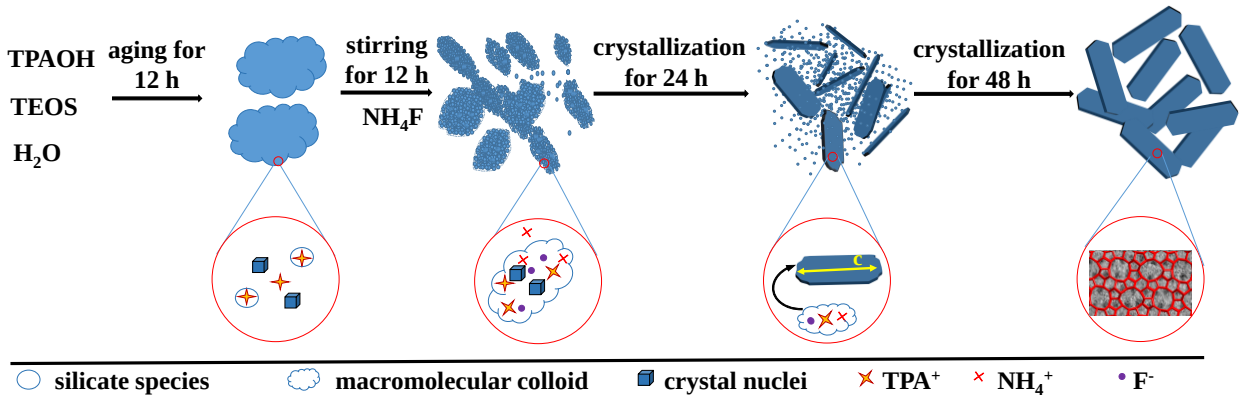

Scheme 1. Schematic presentation of different crystallization stages in the NH_4F-containing system yielding plate-like MFI crystals.

Additional experiments were conducted to reveal the role of NH_4F in the formation of plate-like MFI crystals. NaF and KF were used as fluoride sources to replace NH_4F. The use of both fluoride sources resulted in the formation of oval shape 90° twins with a size of about 1 μm (Figure S15). Since the fluoride content in the systems is similar, the observed effect raises the question about NH_4^+ cation role. Sodium and potassium exhibit a structure-directing effect, and many zeolites are synthesized solely using these two alkali metals. In contrast, ammonium itself cannot generate a zeolite type material due to the weak charge and, consequently, limited interactions with the negatively charged silica species. Hence, we consider ammonium itself does not play an essential role in the growing process and thus does not disturb the formation of plate-like crystallites. Meanwhile, the NH_4F is a buffer that controls the pH. After its addition, the pH of the gel changed from ~12.3 to ~8.5. The introduction of similar molar contents of NaF or KF, adjust the pH value to ~9.7 and ~10.1, respectively. The great decrease of pH value from ~12.3 to ~8.5 certainly decreases the solubility of silicate species, and thus macromolecular colloid species are generated.[51,52] Therefore, the addition of NH_4F has two well-established effects on the initial gel: i) breaking the gel structure and generation of nanoparticles that play an important role in forming plate-like crystals; and ii) decreasing the pH and thus changing the solubility of the silica species. The consequence of these two effects is the preferred growth in *a*- and *c*-directions, owing to the face with the slowest growth rate is the largest,[53] leading to substantial development of the (010) face. The ultimate result is the formation of ultra-thin crystals with a high aspect ratio between different crystal faces. It is worthy to note that the F^- is vital for promoting the

crystallization of MFI zeolite crystals. In a similar synthesis system, where the NH_4Cl replaced NH_4F, only an amorphous product was obtained after two weeks of crystallization (Figure S16).

Silicalite-1 synthesized, according to the present procedure in a mixed OH^-/F^- medium was compared with the counterparts synthesized in OH^- and F^- medium by means of solid-state NMR. The comparative study was based on ^{29}Si MAS, $^{29}Si\{^1H\}$ CPMAS NMR, $^{29}Si\{^{19}F\}$ CPMAS NMR, and ^{19}F MAS NMR analyses. All the samples display resonances in the [–107 ppm; –120 ppm] region corresponding to Q^4 species. However, the sample synthesized in pure F^- medium (Figure S17a3) shows well-resolved peaks corresponding to Q^4 ($Si(OSi)_4$) silicon species, reflecting different crystallographic T positions in MFI-structure. The Q^4 resonances in samples synthesized in a mixed OH^-/F^- (Figure S17a1) and OH^- (Figure S17a2) media are broader because of a less ordered three-dimensional $Si(OSi)_4$ network. This effect is due to local disordering, with a distribution of Si-O-Si angle and distance for each crystallographic silicon T site, leading to a broadening of the well-resolved peaks observed for a high-ordered 3d-network.[54,55] It is even more obvious in the case of OH^- medium synthesized silicalite-1 (Figure S17a2), where almost no discontinuity of the spectral line is observed. In addition, a broad resonance at –103 ppm corresponding to Q^3 ($Si(OSi)_3OH$) is recorded for the silicalite-1 synthesized in mixed (OH^-/F^-) (Figure S17a1 and S17b1) and pure OH^- medium (Figure S17a2 and S17b2). This resonance is a consequence of discontinuity between SiO_4 tetrahedron of the zeolite framework, leading to the formation of Si-OH bonds, and thus defects Q^3. Nevertheless, the fitting of ^{29}Si MAS spectra pointed out a higher amount of defects for silicalite-1 synthesized in OH^- medium (25 %) than for silicalite-1 synthesized in mixed medium (8 %). No Q^3 species are observed in the case of the sample synthesized in NH_4F medium (Figure S17a3), confirmed by no Q^3 signals enhancement in the $^{29}Si\{^1H\}$ CPMAS spectrum (Figure S17b3), indicating a lack of Si-OH defects for this sample and reinforcing the idea of a well-ordered 3d-structure.

Furthermore, a broad peak appears at –125 ppm for the silicalite-1 sample synthesized in F^- medium, which is not observed for the pure OH^- medium synthesized counterpart. This peak is attributed to the fluoride ions, which have certain mobility between $SiO_{4/2}$ tetrahedron. The large signal is typical of framework silicon sites that undergo dynamic exchange between 4- and 5-coordinated environments due to fluoride ion mobility.[56] This signal is not observed in the sample synthesized in mixed (OH^-/F^-)

medium (Figure S17a1 and S17b1). However, this broad resonance at –125 ppm appears and is enhanced by $^{29}Si\{^{19}F\}$ CP transfer (Figure S17c1), suggesting the mobility of F^- ions between $SiO_{4/2}$ tetrahedron. The resonances at –109 and –117 ppm are also broadened slightly by $^{29}Si\{^{19}F\}$ CP process, pointing out that these silicon sites are affected by a disordering of silicon atoms at the vicinity of F^-, or an influence of the mobility of the F^- ion but to a lesser degree. Furthermore, the resonance attributed to Q^3 defects disappears in $^{29}Si\{^{19}F\}$ CPMAS spectrum, in agreement with this assignment.

Figure S18 shows the ^{19}F MAS NMR spectra of silicalite-1 synthesized in NH_4F and mixed (OH^-/F^-) medium (Figure S18a and S18b). The spectrum area in the dotted line is emphasized in the inset. Both spectra exhibit two isotropic signals at –79 ppm and –64 ppm (with a higher intensity for the latter), indicating two environments for fluoride ions. Fits of these spectra show integrated intensities of 99.5 % and 89 % for the main signal for silicalite-1 synthesized in NH_4F and mixed medium, respectively.

The signal at –64 ppm is typical of as-synthesized F-MFI. It is known to result from F^- located in $[4^15^26^2]$ cavity types, where F^- ions are subjected to a dynamic exchange between penta-coordinated Si sites ($[SiO_{4/2}F]^-$).[56–58] The second site at –79 ppm can be due to the SDA (TPA^+) in the straight channels, encountering F^- ions in the cavities. This signal is also attributed to fluorine close to defects. However, the last assignment is in disagreement with the fact that the fluoride medium synthesized silicalite-1 does not contain framework defects, as illustrated in Figure S17b3 ($^{29}Si\{^1H\}$ CPMAS spectrum). Thus, the most plausible interpretation of these two signals would be that there exist two ^{19}F environments, resulting from different interactions of $[SiO_{4/2}F]^-$ with the TPA^+ branches with different conformations in straight and sinusoidal channels.[59] This assignment is also in agreement with other existing studies.[57,60]

Large-scale synthesis of plate-like MFI zeolite

Upscaling synthesis is a challenging and often difficult exercise. A number of parameters are changed when upscale from laboratory to semi-industrial or large scale vessels. For instance, the contact surface between gel and autoclave, heat transfer, concentration gradients, vapor disengagement, and reagent grade.[61] Thus, there exists a large gap between the laboratory-scale synthesis and their industrial implication. Consequently, scale-up is a key problem in zeolite production, which greatly limits the

industrial application of zeolites with various topologies.

The ultra-thin plate-like silicalite-1 can be easily synthesized at low temperature and under ambient pressure, the conditions gracefully suitable to large-scale synthesis. The applicability of our approach to a large scale synthesis was verified by using a 20 L open glass reactor (Figure 4a). The transparent glass reactor allows monitoring the physical changes in the synthesis system, as shown in Figure 4b. Also, the crystallization process in the employed open synthesis system can be easily monitored by sampling at different times. The scale-up experiment was successful, and ~1320 g dry zeolite powder was obtained (Figure 4c, after calcination). The product yield is calculated to be ~97% based on silica conversion, which is impressively high for the large-scale zeolite synthesis. The XRD patterns (Figure 4d) and SEM images (Figure 4e) revealed that the crystallization in the 20 L glass reactor was completed within 96 h, noticeable longer than that in the 20 mL autoclave. This was the only negative effect of the scaled-up synthesis, which we attribute to the slightly lower temperature employed (88±2 versus 90 ^{o}C) and a slower rise of the temperature in the larger vessel. Nevertheless, the quality of the final product was just as good as the counterpart obtained with laboratory equipment (Figure 1 and 4). The result of scaled-up synthesis clearly indicates that the synthesis strategy developed in this work is readily applicable to industrial scale.

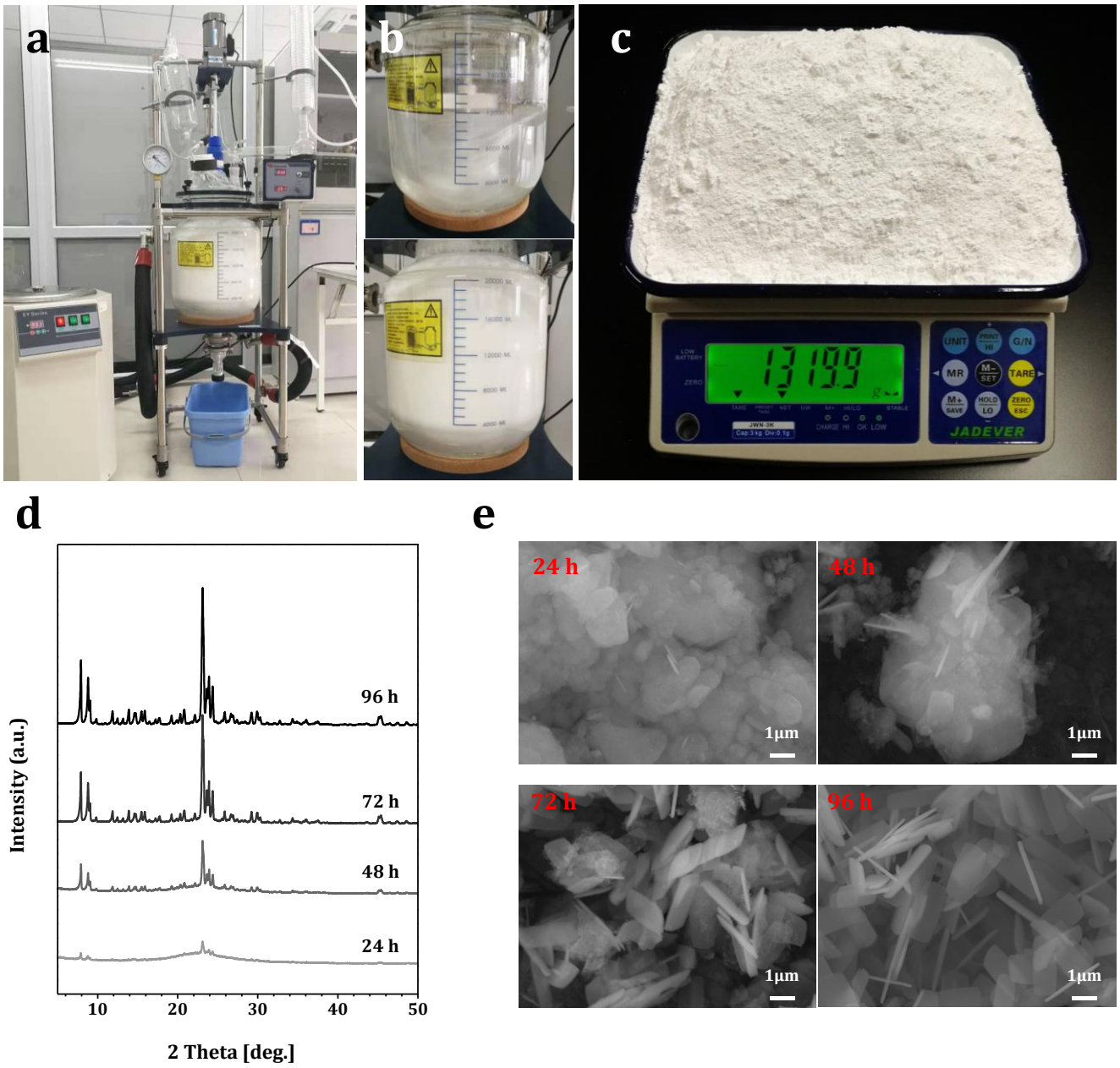

Figure 4. Large-scale syntheses of plate-like MFI zeolite from a gel with composition: 0.1 TPAOH: 1.0 SiO_2: 0.8 NH_4F: 30 H_2O; T = 88±2 ^oC, crystallization time 96 h. (a) Picture of a 20 L glass reactor for large-scale synthesis; (b) Visualization of synthesis process from the initial synthesis gel (upper level) to crystallized product (lower level); (c) Silicalite-1 product after calcination; (d) XRD patterns of solid products obtained after different synthesis time; (e) SEM images of solid products obtained after different synthesis time.

Synthesis of heteroatom-containing plate-like MFI

The catalytic applications of zeolites require the presence of active sites. In this section, we report the synthesis of Al-MFI (ZSM-5) and Ga-MFI counterparts of silicalite-1. The procedure used for the synthesis of plate-like silicalite-1 was employed as a heteroatom was introduced in the initial gel (see Supporting Information for details). Thus a gel with Si/Al ratio 50 was prepared and subjected to hydrothermal treatment at 90 °C. All obtained materials were highly crystalline. The initial gel with Si/Al ratio of 50 yielded crystalline ZSM-5 crystals with Si/Al of 72 (Table S1). The framework Al content did not increase even when an initial gel with Si/Al ratio of 25 was employed. This result pointed out a threshold of the framework Al incorporation under our synthesis conditions. The most plausible reasons limiting the Al incorporation in the ZSM-5 crystals are: i) the presence of F^- ions that compensate the positively charged TPA^+; ii) the absence of alkali cations; and iii) the low synthesis temperature. The synthesized ZSM-5 contained, namely, tetrahedral Al as shown by the dominant resonance at 55 ppm in the ^{27}Al MAS NMR spectrum (Figure S19). The as-obtained plate-like ZSM-5 has similar physicochemical characteristics with the industrial ZSM-5 nanocrystalline sample (Figure S20 and Table S1). Compared with plate-like silicalite-1 crystals, the ZSM-5 counterpart exhibits similar morphology and textural properties (Figure 1c, 5a, S21 and Table S1).

Ga-MFI counterpart of silicalite-1 was also successfully obtained (Figure S22). The materials showed Si/Ga ratio close to 100 (Si/Ga = 98), high crystallinity, and pore volume similar to silicalite-1 synthesized under the same conditions (Table S1). The crystals still exhibited plate-like morphology (Figure S23 and S24), however, compared to the crystals of silicalite-1, smaller crystals with increased thickness along the *b*-axis can be observed. The aspect ratio of L_c/L_b for Ga-MFI was ~10, which is much lower than silicalite-1 synthesized under the same conditions.

Catalytic performance of plate-like ZSM-5 in the MTH reaction

Methanol-to-hydrocarbons (MTH) is often used as a important model reaction for exploring the improved diffusion behaviors of morphology-controlled zeolite catalysts.[62,63] Herein, the catalytic performance of plate-like HZSM-5 crystals, in comparison with commercial ZSM-5 nanocrystals with a similar number of Brønsted acid sites (Table S1), was evaluated in the MTH reaction. As shown in Figure 5b, plate-like HZSM-5 samples exhibit an ultra-long lifetime of 250 h (methanol

conversion >99%), which is five times longer than that of commercial ZSM-5 nanocrystals under identical reaction conditions. The extended lifetime is attributed to the shorter diffusion path along the straight channel of ZSM-5 crystals. The plate-like crystals of thickness around 100 nm improve the mass transfer significantly and slow down the coke accumulation. According to the time-dependent product distribution in MTH reaction (Figure 5c-d), higher propylene selectivity (~30% versus ~26%) but lower BTX selectivity (~14% versus ~17%) was obtained on plate-like ZSM-5 samples in comparison with commercial ZSM-5 nanocrystals, as a result of the diffusion control. Therefore, the plate-like HZSM-5 is a high performing acid catalyst for the industrial MTH reaction, and it also holds promises for other catalytic applications, especially when dealing with bulky molecules.[8]

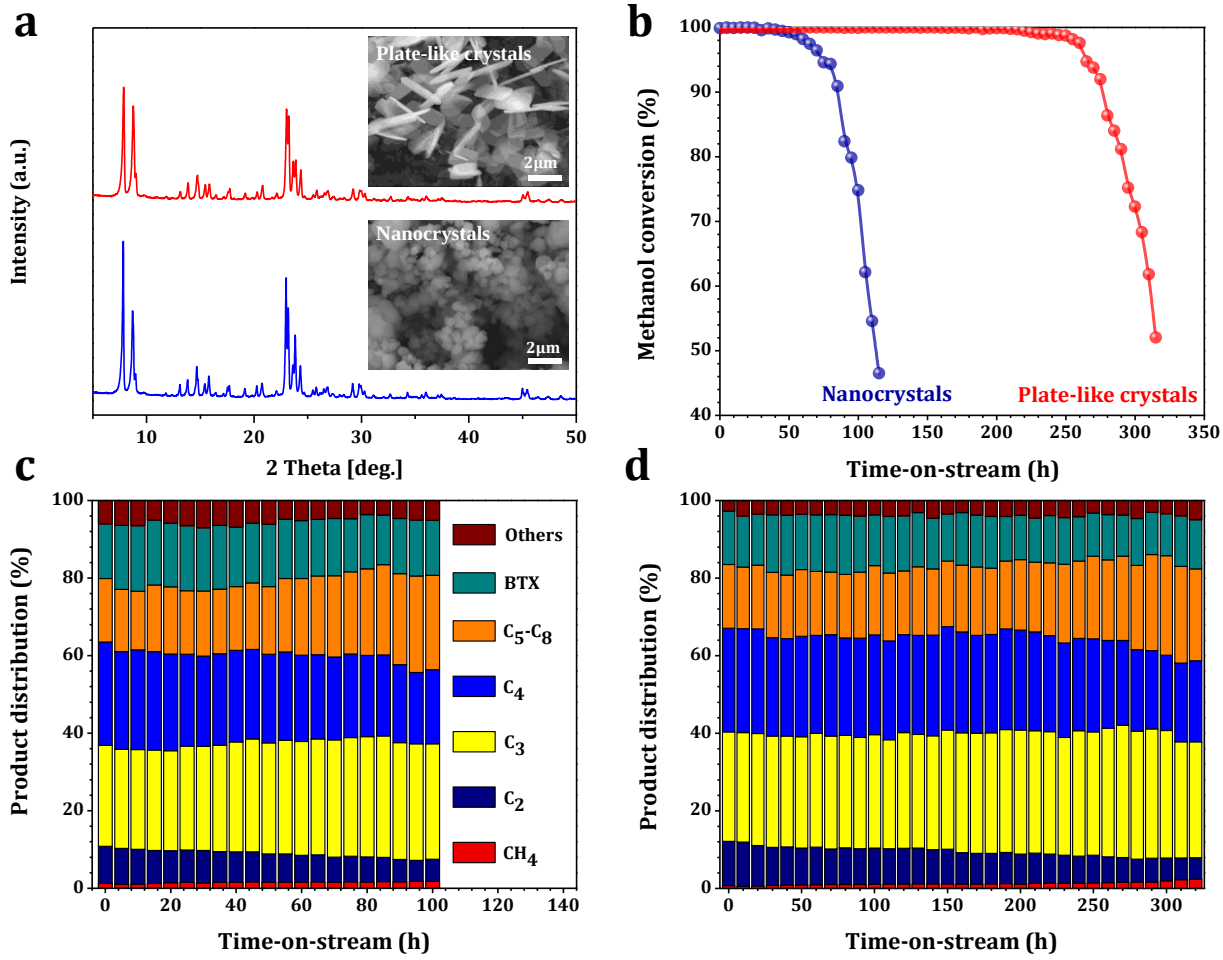

Figure 5. Comparative study of the MTH performance of plate-like HZSM-5 crystals and commercial ZSM-5 nanocrystals: (a) XRD patterns of calcined plate-like HZSM-5 (top, Si/Al = 72) and commercial ZSM-5 nanocrystals (bottom, Si/Al = 74); Inset: representative SEM images of solid products; (b) Methanol conversion as a function of reaction time over two different ZSM-5 samples; Product

selectivity as a function of time over commercial ZSM-5 nanocrystals (c) and plate-like HZSM-5 (d) in MTH reaction. Reaction conditions: 0.4 g catalyst, WHSV = 2 h^{-1}, T = 425 °C, ambient pressure.

Conclusions

A synthetic approach yielding ultra-thin plate-like MFI-type crystals without using special structure-directing reagents or organic growth-modifiers is developed. The crystal thickness along the straight channel (*b*-axis) can be effectively tuned to several tens of nm, thus shortening the diffusion path. This simple approach also allows tuning the aspect ratio between different crystal faces, thus developing the crystal face with the channel system of interest. Consequently, the number of pore openings per unit crystal surface is maximized, and the diffusion limitations' impact is minimized.

The synthetic approach combines preliminary aging in F-free medium with a fluoride-assisted low-temperature crystallization process. Thus the nucleation process is split from the crystallization, which takes place in F-containing medium. A suitable aging time (12 h) is indispensable for the formation of viable MFI nuclei, while the crystallization is controlled by the presence of fluorine mineralizer. The specific effect of F^- on the precursor gel structure, the pH of the gel, and thus the solubility of the silica species, resulting in an alteration of the growing mechanism, leads to the formation of ultra-thin crystals with high L_c/L_b aspect ratio.

The above-described synthesis strategy is versatile, efficient, and applicable for the industrial production of plate-like zeolites. We have obtained a similar result, i.e., ultra-thin plate-like FER-type zeolite (Figure S25), which proves that a general strategy applicable to different zeolite types is developed. It can be scaled up for the synthesis of kilogram-scale siliceous MFI zeolites in an open glass reactor with an extremely high yield of ~97%, and it can also be extended to the synthesis of heteroatom containing MFI zeolites like Al-MFI and Ga-MFI.

Associated content

Supporting information

The supporting information is available for this paper, including Materials and Methods, Figures S1-S25 and Table S1.

Author information

Corresponding Author:

*E-mail: wuguangjun@nankai.edu.cn (G.W.);

*E-mail: valentin.valtchev@ensicaen.fr (V.V.).

ORCID：

Valentin Valtchev: 0000-0002-2341-6397

Notes

The authors declare no competing financial interests.

Acknowledgments

We acknowledge the National Natural Science Funds of China (21722303, 22025203), the Municipal Natural Science Funds of Tianjin (18JCJQJC47400), 111 Project (B18030), and the China Scholarship Council for supporting the work. V.V. acknowledges the financial support from the Industrial Chair ANR-TOTAL "NanoClean Energy" (ANR-17-CHIN-0005-01) and FEDER 18P01675.

References

(1) Barrer, R. M. *Hydrothermal Chemistry of Zeolites*; London, 1982.

(2) Milton, R. M. *Molecular Sieve Science and Technology, A Historical Perspective*; Washington, DC,1989.

(3) Breck, D. W. *Zeolite Molecular Sieves: Structure, Chemistry and Use*, Wiley: New York, 1974.

(4) Na, K.; Choi, M.; Ryoo, R. Recent Advances in the Synthesis of Hierarchically Nanoporous Zeolites. *Micropor. Mesopor. Mater.* **2013**, *166*, 3–19.

(5) Hartmann, M.; Machoke, A. G.; Schwieger, W. Catalytic Test Reactions for the Evaluation of Hierarchical Zeolites. *Chem. Soc. Rev.* **2016**, *45*, 3313–3330.

(6) Wei, Y.; Parmentier, T. E.; De Jong, K. P.; Zečević, J. Tailoring and Visualizing the Pore Architecture of Hierarchical Zeolites. *Chem. Soc. Rev.* **2015**, *44*, 7234–7261.

(7) Guisnet, M.; Ribeiro, F. R. Deactivation and Regeneration of Solid Catalysts; Imperial College Press, London, 2011.

(8) Choi, M.; Na, K.; Kim, J.; Sakamoto, Y.; Terasaki, O.; Ryoo, R. Stable Single-Unit-Cell Nanosheets of Zeolite MFI as Active and Long-Lived Catalysts. *Nature* **2009**, *461*, 246–249.

(9) Valtchev, V.; Tosheva, L. Porous Nanosized Particles : Preparation, Properties, and Applications. *Chem. Rev.* **2013**, *113*, 6734–6760.

(10) Mintova, S.; Jaber, M.; Valtchev, V. Nanosized Microporous Crystals: Emerging Applications. *Chem. Soc. Rev.* **2015**, *44*, 7207–7233.

(11) Mintova, S.; Gilson, J. P.; Valtchev, V. Advances in Nanosized Zeolites. *Nanoscale* **2013**, *5*, 6693–6703.

(12) Tosheva, L.; Valtchev, V. P. Nanozeolites: Synthesis, Crystallization Mechanism, and Applications. *Chem. Mater.* **2005**, *17*, 2494–2513.

(13) Möller, K.; Bein, T. Mesoporosity – a New Dimension for Zeolites. *Chem. Soc. Rev.* **2013**, *42*, 3689–3707.

(14) Serrano, D. P.; Escola, J. M.; Pizarro, P. Synthesis Strategies in the Search for Hierarchical Zeolites. *Chem. Soc. Rev.* **2013**, *42*, 4004–4035.

(15) Tao, Y.; Kanoh, H.; Abrams, L.; Kaneko, K. Mesopore-Modified Zeolites : Preparation, Characterization, and Applications. *Chem. Rev.* **2006**, *106*, 896–910.

(16) Holm, M. S.; Taarning, E.; Egeblad, K.; Christensen, C. H. Catalysis with Hierarchical Zeolites. *Catal. Today* **2011**, *168*, 3–16.

(17) Meng, L.; Zhu, X.; Mezari, B.; Pestman, R.; Wannapakdee, W.; Hensen, E. J. M. On the Role of Acidity in Bulk and Nanosheet [T]MFI (T=Al^{3+}, Ga^{3+}, Fe^{3+}, B^{3+}) Zeolites in the Methanol-to-Hydrocarbons Reaction. *ChemCatChem* **2017**, *9*, 3942–3954.

(18) Liu, Y.; Qiang, W.; Ji, T.; Zhang, M.; Li, M.; Lu, J.; Liu, Y. Uniform Hierarchical MFI Nanosheets Prepared via Anisotropic Etching for Solution-Based Sub-100-nm Thick Oriented MFI Layer Fabrication. *Sci. Adv.* **2020**, *6*, 1–9.

(19) Xiao, X.; Zhang, Y.; Jiang, G.; Liu, J.; Han, S.; Zhao, Z.; Wang, R.; Li, C.; Xu, C.; Duan, A.; Wang, Y.; Liu, J.; Wei, Y. Simultaneous Realization of High Catalytic Activity and Stability for Catalytic Cracking of: N -Heptane on Highly Exposed (010) Crystal Planes of Nanosheet ZSM-5 Zeolite. *Chem. Commun.* **2016**, *52*, 10068–10071.

(20) Jeon, M. Y.; Kim, D.; Kumar, P.; Lee, P. S.; Rangnekar, N.; Bai, P.; Shete, M.; Elyassi, B.; Lee, H. S.; Narasimharao, K.; Basahel, S. N.; Al-Thabaiti, S.; Xu, W.; Cho, H. J.; Fetisov, E. O.; Thyagarajan, R.; Dejaco, R. F.; Fan, W.; Mkhoyan, K. A.; Siepmann, J. I.; Tsapatsis, M. Ultra-Selective High-Flux Membranes from Directly Synthesized Zeolite Nanosheets. *Nature* **2017**, *543*, 690–694.

(21) Hu, S.; Shan, J.; Zhang, Q.; Wang, Y.; Liu, Y.; Gong, Y.; Wu, Z.; Dou, T. Selective Formation of Propylene from Methanol over High-Silica Nanosheets of MFI Zeolite. *Appl. Catal., A.* **2012**, *445–446*, 215–220.

(22) Ji, Y.; Shi, B.; Yang, H.; Yan, W. Synthesis of Isomorphous MFI Nanosheet Zeolites for Supercritical Catalytic Cracking of n-Dodecane. *Appl. Catal., A.* **2017**, *533*, 90–98.

(23) Seo, Y.; Cho, K.; Jung, Y.; Ryoo, R. Characterization of the Surface Acidity of MFI Zeolite Nanosheets by ^{31}P NMR of Adsorbed Phosphine Oxides and Catalytic Cracking of Decalin. *ACS Catal.* **2013**, *3*, 713–720.

(24) Xu, M.; Mukarakate, C.; Iisa, K.; Budhi, S.; Menart, M.; Davidson, M.; Robichaud, D. J.; Nimlos, M. R.; Trewyn, B. G.; Richards, R. M. Deactivation of Multilayered MFI Nanosheet Zeolite during Upgrading of Biomass Pyrolysis Vapors. *ACS Sustain. Chem. Eng.* **2017**, *5*, 5477–5484.

(25) Kim, J.; Park, W.; Ryoo, R. Surfactant-Directed Zeolite Nanosheets: A High-Performance Catalyst for Gas-Phase Beckmann Rearrangement. *ACS Catal.* **2011**, *1*, 337–341.

(26) Kim, D.; Jeon, M. Y.; Stottrup, B. L.; Tsapatsis, M. Para-Xylene Ultra-Selective Zeolite MFI Membranes Fabricated from Nanosheet Monolayers at the Air-Water Interface. *Angew. Chem. Int. Ed.* **2018**, *57*, 480–485.

(27) Zhang, H.; Xiao, Q.; Guo, X.; Li, N.; Kumar, P.; Rangnekar, N.; Jeon, M. Y.; Al-Thabaiti, S.; Narasimharao, K.; Basahel, S. N.; Topuz, B.; Onorato, F. J.; Macosko, C. W.; Mkhoyan, K. A.; Tsapatsis, M. Open-Pore Two-Dimensional MFI Zeolite Nanosheets for the Fabrication of

Hydrocarbon-Isomer-Selective Membranes on Porous Polymer Supports. *Angew. Chem. Int. Ed.* **2016**, *55*, 7184–7187.

(28) Na, K.; Park, W.; Seo, Y.; Ryoo, R. Disordered Assembly of MFI Zeolite Nanosheets with a Large Volume of Intersheet Mesopores. *Chem. Mater.* **2011**, *23*, 1273–1279.

(29) Na, K.; Chol, M.; Park, W.; Sakamoto, Y.; Terasakl, O.; Ryoo, R. Pillared MFI Zeolite Nanosheets of a Single-Unit-Cell Thickness. *J. Am. Chem. Soc.* **2010**, *132*, 4169–4177.

(30) Shen, X.; Mao, W.; Ma, Y.; Xu, D.; Wu, P.; Terasaki, O.; Han, L.; Che, S. A Hierarchical MFI Zeolite with a Two- Dimensional Square Mesostructure. *Angew. Chem. Int. Ed* **2018**, *57*, 724–728.

(31) Maheshwari, S.; Jordan, E.; Kumar, S.; Bates, F. S.; Penn, R. L.; Shantz, D. F.; Tsapatsis, M. Layer Structure Preservation during Swelling, Pillaring, and Exfoliation of a Zeolite Precursor. *J. Am. Chem. Soc.* **2008**, *130*, 1507–1516.

(32) Itani, L.; Bozhilov, K. N.; Clet, G.; Delmotte, L.; Valtchev, V. Factors That Control Zeolite L Crystal Size. *Chem. Eur. J.* **2011**, *17*, 2199–2210.

(33) Larlus, O.; Valtchev, V. P. Crystal Morphology Control of LTL-Type Zeolite Crystals. *Chem. Mater.* **2004**, *16*, 3381–3389.

(34) Zhang, Q.; Mayoral, A.; Terasaki, O.; Zhang, Q.; Ma, B.; Zhao, C.; Yang, G.; Yu, J. Amino Acid-Assisted Construction of Single-Crystalline Hierarchical Nanozeolites via Oriented-Aggregation and Intraparticle Ripening. *J. Am. Chem. Soc.* **2019**, 3772–3776.

(35) Larlus, O.; Valtchev, V. P. Control of the Morphology of All-Silica BEA-Type Zeolite Synthesized in Basic Media. *Chem. Mater.* **2005**, *17*, 881–886.

(36) Li, S.; Li, J.; Dong, M.; Fan, S.; Zhao, T.; Wang, J.; Fan, W. Strategies to Control Zeolite Particle Morphology. *Chem. Soc. Rev.* **2019**, *48*, 885–907.

(37) Zhang, Q.; Chen, G.; Wang, Y.; Chen, M.; Guo, G.; Shi, J.; Luo, J.; Yu, J. High-Quality Single-Crystalline MFI-Type Nanozeolites: A Facile Synthetic Strategy and MTP Catalytic Studies. *Chem. Mater.* **2018**, *30*, 2750–2758.

(38) Chen, X.; Yan, W.; Cao, X.; Yu, J.; Xu, R. Fabrication of Silicalite-1 Crystals with Tunable Aspect Ratios by Microwave-Assisted Solvothermal Synthesis. *Micropor. Mesopor. Mater.* **2009**,

119, 217–222.

(39) Lupulescu, A. I.; Kumar, M.; Rimer, J. D. A Facile Strategy to Design Zeolite L Crystals with Tunable Morphology and Surface Architecture. *J. Am. Chem. Soc.* **2013**, *135*, 6608–6617.

(40) Lupulescu, A. I.; Rimer, J. D. Tailoring Silicalite-1 Crystal Morphology with Molecular Modifiers. *Angew. Chem. Int. Ed.* **2012**, *51*, 3345–3349.

(41) Li, H.; Liu, X.; Qi, S.; Xu, L.; Shi, G.; Ding, Y.; Yan, X.; Huang, Y.; Geng, J. Graphene Oxide Facilitates Solvent-Free Synthesis of Well-Dispersed, Faceted Zeolite Crystals. *Angew. Chem. Int. Ed.* **2017**, *56*, 14090–14095.

(42) Li, R.; Smolyakova, A.; Maayan, G.; Rimer, J. D. Designed Peptoids as Tunable Modifiers of Zeolite Crystallization. *Chem. Mater.* **2017**, *29*, 9536–9546.

(43) Qin, W.; Agarwal, A.; Choudhary, M. K.; Palmer, J. C.; Rimer, J. D. Molecular Modifiers Suppress Nonclassical Pathways of Zeolite Crystallization. *Chem. Mater.* **2019**, *31*, 3228–3238.

(44) Kessler, H.; Patarin, J.; Schott-Darie, C. *The Opportunities of the Fluoride Route in the Synthesis of Microporous Materials*; *Stud. Surf. Sci. Catal*. **1994**; *85*, 75-113.

(45) Caullet, P.; Paillaud, J. L.; Simon-Masseron, A.; Soulard, M.; Patarin, J. The Fluoride Route: A Strategy to Crystalline Porous Materials. *C. R. Chim.* **2005**, *8*, 245–266.

(46) Zhou, M.; Korelskiy, D.; Ye, P.; Grahn, M.; Hedlund, J. A Uniformly Oriented MFI Membrane for Improved CO_2 Separation. *Angew. Chem. Int. Ed.* **2014**, *53*, 3492–3495.

(47) Pereira, M. M.; Gomes, E. S.; Silva, A. V.; Pinar, A. B.; Willinger, M. G.; Shanmugam, S.; Chizallet, C.; Laugel, G.; Losch, P.; Louis, B. Biomass-Mediated ZSM-5 Zeolite Synthesis: When Self-Assembly Allows to Cross the Si/Al Lower Limit. *Chem. Sci.* **2018**, *9*, 6532–6539.

(48) Kirschhock, C. E. A.; Ravishankar, R.; Verspeurt, F.; Grobet, P. J.; Jacobs, P. A.; Martens, J. A. Identification of Precursor Species in the Formation of MFI Zeolite in the TPAOH-TEOS-H_2O System. *J. Phys. Chem. B* **1999**, *103*, 4965–4971.

(49) Li, Q.; Mihailova, B.; Creaser, D.; Sterte, J. Aging Effects on the Nucleation and Crystallization Kinetics of Colloidal TPA-Silicalite-1. *Micropor. Mesopor. Mater.* **2001**, *43*, 51–59.

(50) Grand, J.; Awala, H.; Mintova, S. Mechanism of Zeolites Crystal Growth: New Findings and Open Questions. *CrystEngComm* **2016**, *18*, 650–664.

(51) Lesthaeghe, D.; Vansteenkiste, P.; Verstraelen, T.; Ghysels, A.; Kirschhock, C. E. A.; Martens, J. A.; Van Speybroeck, V.; Waroquier, M. MFI Fingerprint: How Pentasil-Induced IR Bands Shift during Zeolite Nanogrowth. *J. Phys. Chem. C* **2008**, *112*, 9186–9191.

(52) Fan, W.; Duan, R. G.; Yokoi, T.; Wu, P.; Kubota, Y.; Tatsumi, T. Synthesis, Crystallization Mechanism, and Catalytic Properties of Titanium-Rich TS-1 Free of Extraframework Titanium Species. *J. Am. Chem. Soc.* **2008**, *130*, 10150–10164.

(53) Sunagawa, I. *Crystals: Growth, Morphology, and Perfection*; Cambridge University Press, Cambridge, UK, 2005.

(54) Fyfe, C. A.; Grondey, H.; Feng, Y.; Kokotailo, G. T. Natural-Abundance Two-Dimensional ^{29}Si MAS NMR Investigation of the Three-Dimensional Bonding Connectivities in the Zeolite Catalyst ZSM-5. *J. Am. Chem. Soc.* **1990**, *112*, 8812–8820.

(55) Cadars, S.; Brouwer, D. H.; Chmelka, B. F. Probing Local Structures of Siliceous Zeolite Frameworks by Solid-State NMR and First-Principles Calculations of ^{29}Si-O-^{29}Si Scalar Couplings. *Phys. Chem. Chem. Phys.* **2009**, *11*, 1825–1837.

(56) Koller, H.; Wölker, A.; Villaescusa, L. A.; Díaz-Cabañas, M. J.; Valencia, S.; Camblor, M. A. Five-Coordinate Silicon in High-Silica Zeolites. *J. Am. Chem. Soc.* **1999**, *121*, 3368–3376.

(57) Fyfe, C. A.; Brouwer, D. H.; Lewis, A. R.; Chézeau, J. M. Location of the Fluoride Ion in Tetrapropylammonium Fluoride Silicalite-1 Determined by ^{1}H/^{19}F/^{29}Si Triple Resonance CP, REDOR, and TEDOR NMR Experiments. *J. Am. Chem. Soc.* **2001**, *123*, 6882–6891.

(58) Dib, E.; Gimenez, A.; Mineva, T.; Alonso, B. Preferential Orientations of Structure Directing Agents in Zeolites. *Dalt. Trans.* **2015**, *44*, 16680–16683.

(59) Rojas, A.; Gómez-Hortigüela, L.; Camblor, M. A. Zeolite Structure Direction by Simple Bis(Methylimidazolium) Cations: The Effect of the Spacer Length on Structure Direction and of the Imidazolium Ring Orientation on the ^{19}F NMR Resonances. *J. Am. Chem. Soc.* **2012**, *134*, 3845–3856.

(60) Dib, E.; Mineva, T.; Gaveau, P.; Alonso, B. ^{14}N Solid-State NMR: A Sensitive Probe of the Local Order in Zeolites. *Phys. Chem. Chem. Phys.* **2013**, *15*, 18349–18352.

(61) Hendershot, D. C.; Sarafin, A. Safe Chemical Reaction Scale Up. *Chem. Heal. Saf.* **2005**, *12*,

29–35.

(62) Gallego, E. M.; Paris, C.; Díaz-Rey, M. R.; Martínez-Armero, M. E.; Martínez-Triguero, J.; Martínez, C.; Moliner, M.; Corma, A. Simple Organic Structure Directing Agents for Synthesizing Nanocrystalline Zeolites. *Chem. Sci.* **2017**, *8*, 8138–8149.

(63) Dai, H.; Shen, Y.; Yang, T.; Lee, C.; Fu, D.; Agarwal, A.; Le, T. T.; Tsapatsis, M.; Palmer, J. C.; Weckhuysen, B. M.; Dauenhauer, P. J.; Zou, X.; Rimer, J. D. Finned Zeolite Catalysts. *Nat. Mater.* **2020**, *19*, 1074–1080.

Table of Contents Graphic